# Electronic nematicity in $Sr_2RuO_4$

Jie Wu[a,1,2], Hari P. Nair[b,1], Anthony T. Bollinger[a], Xi He[a,c], Ian Robinson[a], Nathaniel J. Schreiber[b], Kyle M. Shen[d,e], Darrell G. Schlom[b,e], and Ivan Božović[a,c,3]

[a]Brookhaven National Laboratory, Upton, NY 11973-5000; [b]Department of Materials Science and Engineering, Cornell University, Ithaca, NY 14853; [c]Department of Chemistry, Yale University, New Haven CT 06520; [d]Physics Department, Cornell University, Ithaca, NY 14853; and [e]Kavli Institute at Cornell for Nanoscale Science, Ithaca, NY 14853

Edited by Zachary Fisk, University of California, Irvine, CA, and approved March 25, 2020 (received for review December 10, 2019)

**We have measured the angle-resolved transverse resistivity (ARTR), a sensitive indicator of electronic anisotropy, in high-quality thin films of the unconventional superconductor $Sr_2RuO_4$ grown on various substrates. The ARTR signal, heralding the electronic nematicity or a large nematic susceptibility, is present and substantial already at room temperature and grows by an order of magnitude upon cooling down to 4 K. In $Sr_2RuO_4$ films deposited on tetragonal substrates the highest-conductivity direction does not coincide with any crystallographic axis. In films deposited on orthorhombic substrates it tends to align with the shorter axis; however, the magnitude of the anisotropy stays the same despite the large lattice distortion. These are strong indications of actual or incipient electronic nematicity in $Sr_2RuO_4$.**

electronic nematicity | strontium ruthenate | molecular-beam epitaxy | angle-resolved transverse resistivity

It has been predicted theoretically that in some unconventional metals the symmetry of the electron fluid can be spontaneously broken, i.e., reduced compared to that of the underlying crystal lattice (1–5). Indeed, transport anisotropy unexpected from the crystal structure has been observed in copper-oxide (6–15), Fe-based (16–19), and heavy-fermions superconductors (20, 21). This situation is frequently referred to as "electronic nematicity." Here, we will use this term as a shorthand for transport anisotropy that predominantly originates from within the electron fluid itself, i.e., from electron–electron interactions.[†] This brings into focus the interplay between unconventional superconductivity, nematicity, and electron correlations.

Our recent study of a prototypical *d*-wave superconductor, $La_{2-x}Sr_xCuO_4$, using the angle-resolved transverse resistivity (ARTR) method (15), revealed that the electric transport in the normal state shows only twofold rotational symmetry ($\mathbf{C_2}$) while the tetragonal crystal lattice has higher, fourfold ($\mathbf{C_4}$) symmetry. This deviation from the canonical Fermi liquid behavior in cuprates has been ascribed to strong electron correlations. It is of fundamental interest to explore how widespread the nematic state is and whether it is linked with unconventional superconductivity. We have chosen to start with $Sr_2RuO_4$, since it also is an unconventional superconductor, harbors strong electron correlations, and has the same layered-perovskite ($K_2NiF_4$) structure as $La_{2-x}Sr_xCuO_4$ (22–30). Thus, one wonders whether the normal state of $Sr_2RuO_4$, from which the superconductivity emerges, also breaks the rotational symmetry of the lattice, or not.

With this motivation, we have synthesized high-quality single-crystal films of (001)-oriented $Sr_2RuO_4$ by molecular-beam epitaxy (30). The best films are superconducting with critical temperature $T_c \sim 1.5$ K. The films are deposited on (001)-oriented $(LaAlO_3)_{0.29}$—$(SrTa_{1/2}Al_{1/2}O_3)_{0.71}$ (LSAT) and (110)-oriented $NdGaO_3$ substrates.[‡] The film thickness is chosen to be smaller than the critical thickness for the onset of relaxation, so the in-plane lattice constants of the films remain the same as those of the underlying substrate. Since LSAT is tetragonal while $NdGaO_3$ is orthorhombic (31), comparing $Sr_2RuO_4$/LSAT to $Sr_2RuO_4$/$NdGaO_3$ enables us to discern the contributions of the lattice distortion to the observed effects. Details on the synthesis as well as the structural and morphological characterization of the films are provided in *SI Appendix*.

To study the nematicity, we have developed a direct and sensitive method, ARTR (15). The lithography pattern we use is depicted in Fig. 1*A*. A total of 36 Hall bars are arranged radially in a "sunbeam" pattern, with $\Delta\phi = 10°$ angles between successive Hall bars. The electric current runs along a Hall bar, while longitudinal or transverse voltages are measured using three pairs of evenly spaced gold contacts, Fig. 1*B*. The angle $\phi = 0°$ corresponds to the [100] direction of the $Sr_2RuO_4$ lattice. As explained in ref. 15, if the crystal and the electron fluid both have tetragonal ($\mathbf{C_4}$) symmetry in-plane, the longitudinal resistivity $\rho$ must be isotropic, and the transverse resistivity $\rho_T$ must be zero by symmetry at every angle. In contrast, if the symmetry of the electron transport is reduced to $\mathbf{C_2}$, $\rho_T$ must be nonzero except when the current flow is along one of the principal axes of the electrical conductivity tensor. More precisely, both $\rho$ and $\rho_T$ must oscillate as a function of $\phi$ with the period of 180°, as follows:

## Significance

**We have synthesized high-quality thin films of the unconventional superconductor $Sr_2RuO_4$ on various substrates using molecular-beam epitaxy. We have measured the angle-resolved transverse resistivity (ARTR), a sensitive indicator of electronic anisotropy. The ARTR signal, heralding the electronic nematicity or a large nematic susceptibility, is present and substantial already at room temperature and grows by an order of magnitude upon cooling down to 4 K. In $Sr_2RuO_4$, an unconventional superconducting state emerges out of an unconventional metallic state.**

Author contributions: K.M.S., D.G.S., and I.B. designed research; J.W., H.P.N., A.T.B., X.H., I.R., N.J.S., and I.B. performed research; K.M.S., D.G.S., and I.B. analyzed data; and D.G.S. and I.B. wrote the paper.

The authors declare no competing interest.

This article is a PNAS Direct Submission.



[1]J.W. and H.P.N. contributed equally to this work.

[2]Present address: Department of Physics, Westlake University, 310024 Hangzhou, Zhejiang, People's Republic of China.

[3]To whom correspondence may be addressed. Email: bozovic@bnl.gov.

This article contains supporting information online at https://www.pnas.org/lookup/suppl/doi:10.1073/pnas.1921713117/-/DCSupplemental.

First published May 4, 2020.

[†]This differentiates "electronic nematicity" from transport anisotropy that predominantly originates from the orthorhombicity of the crystal structure, or from formation of a charge density wave that originates from the electron–phonon interaction. In an electronic nematic, both of these effects must be present in principle, but they need not be dominant, and may even be negligible.

[‡]The indices used (also by the substrate vendor) for the $NdGaO_3$ substrate refer to orthorhombic indices (*Pbnm* setting), where the long axis of $NdGaO_3$ is the [001] direction. Similarly, LSAT is referred to with pseudocubic indices even though it is in fact tetragonal, but the distortion is so small that it is difficult to discern and is generally ignored.

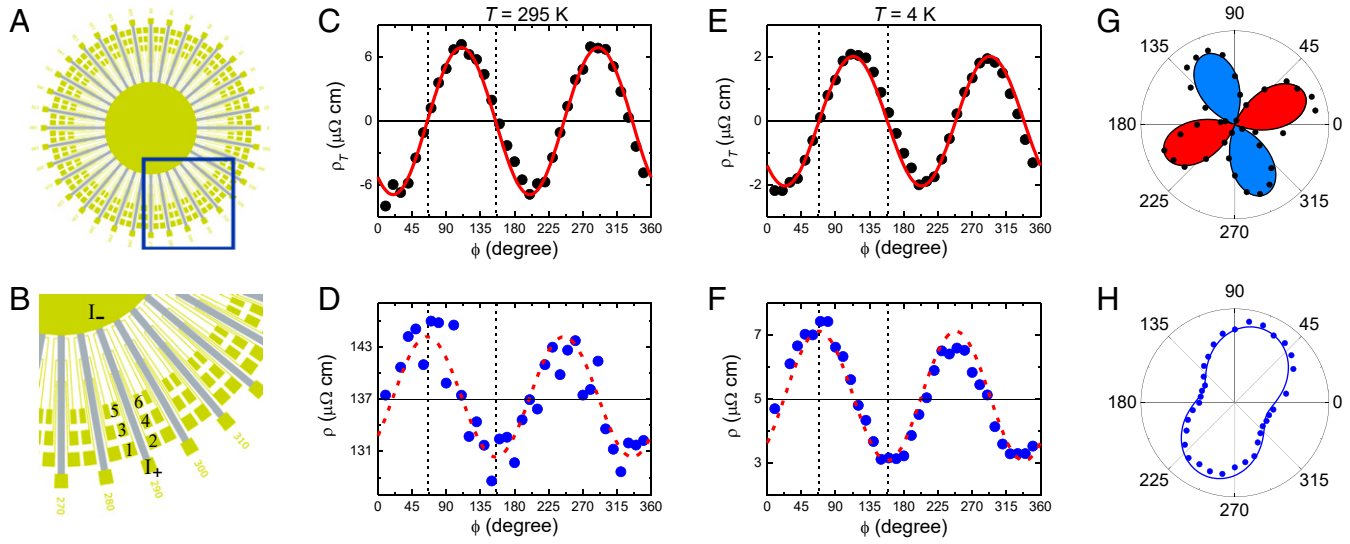


**Fig. 1.** Angular dependence of the transverse ($\rho_T$) and longitudinal ($\rho$) resistivity of the tetragonal $Sr_2RuO_4$ film on the LSAT substrate. In ultrathin $Sr_2RuO_4$ films, as determined by the high-resolution X-ray diffraction experiments, the in-plane lattice constants *a* and *b* are epitaxially anchored to those of the substrate. Their difference is tiny (less than 0.03%) in $Sr_2RuO_4$ grown on tetragonal LSAT substrates. (*A*) A schematic drawing of the lithographic pattern used in this study. Thirty-six identical Hall bars are drawn in steps of $\Delta\phi = 10°$ to cover the whole range from 0 to 360°. (*B*) On each Hall bar, the current runs from the contact I+ to the contact I–. The longitudinal voltages are recorded using pairs like {1,3} and {3,5}, and the transverse voltages using the pairs {1,2}, {3,4}, and {5,6}. The film thickness is 23 nm, the width of each strip is 100 μm, and the voltage contacts are spaced 300 μm apart. (*C*) The measured transverse resistivity $\rho_T$ (black dots) at $T =$ 295 K fits well (the solid red curve) to $\rho_T(\phi) = \rho_T{}^0\sin[2(\phi-\alpha)]$, with $\alpha = 65°$. The black dashed lines mark the angles at which $\rho_T(\phi)$ cross zero. (*D*) The measured longitudinal resistivity $\rho(\phi)$ (blue dots) at $T = 295$ K is well reproduced (the dashed red line) by shifting the fit $\rho_T(\phi)$ curve upward by a constant, $\bar{\rho}$, and left by 45°. The black dashed lines are aligned with those in *C* and correspond to the angles at which $\rho(\phi)$ manifests maximum or minimum values, evidencing the correlation between $\rho_T(\phi)$ and $\rho(\phi)$. (*E*) The same as in *C* but for $T = 4$ K. (*F*) The same as in *D* but for $T = 4$ K. (*G*) The same as in *E*, but plotted in polar coordinates; the experimental data (black dots) and the fit curve (the solid line). Blue filling indicates positive and red negative values. (*H*) The same as in *F*, in polar coordinates.

$$\rho(\phi) = \bar{\rho} + \Delta\rho\cos[2(\phi - a)], \quad [1]$$

$$\rho_T(\phi) = \rho_T^0\sin[2(\phi - a)], \quad [2]$$

where $\bar{\rho} = (\rho_{max} + \rho_{min})/2$, the largest resistivity $\rho_{max}$ is measured along the "hard" axis oriented at some angle $\alpha$, the smallest resistivity $\rho_{min}$ is measured along the "easy" axis at $\phi = \alpha \pm 90°$, and $\rho_T{}^0 = \Delta\rho = (\rho_{max} - \rho_{min})/2$.

Hence, by measuring $\rho_T(\phi)$ one can detect the breaking of the fourfold symmetry of $Sr_2RuO_4$. Note that while $\rho(\phi)$ oscillates around some average value $\bar{\rho}$ that can be large, $\rho_T(\phi)$ oscillates around zero and is thus free of such a background signal. This makes the ARTR measurements much more sensitive to the electronic nematicity; its signal-to-noise (limited by the inevitable device-to-device variations due to lithography) is typically better than that of measurements of $\rho(\phi)$ by about 2 orders of magnitude. This ARTR method has substantial advantages compared to just measuring the longitudinal resistivity $\rho_a$ and $\rho_b$ along the two in-plane crystallographic directions, e.g., [100] and [010]. This is best illustrated by an example where the easy axis is diagonal, $\alpha = 45°$. Then one would measure $\rho_a = \rho_b = \bar{\rho}$ and conclude that the sample is isotropic, even if $\rho_{max}$ and $\rho_{min}$ in fact differ by orders of magnitude. In any case, the angular resolution is crucial for determining the principal axes of the resistivity tensor in the event that the tetragonal symmetry is broken and the in-plane resistivity is no longer isotropic. Note that if the symmetry is reduced to orthorhombic, the principal axes of the resistivity tensor must still be aligned with the crystallographic axes, but for lower symmetries are no longer constrained. Importantly, the current flow in the sunbeam pattern is guided in the direction defined by the in-plane orientation of the Hall bar. This is not the case in, e.g., the van der Pauw method (32) where the current flow pattern gets distorted toward the easy axis; this complicates the analysis and can easily produce spurious sign reversals of the $\rho_a/\rho_b$ ratio, as we illustrate in *SI Appendix*.

Our measurements made with the ARTR technique are inconsistent with the fourfold symmetry $Sr_2RuO_4$ is believed to possess (33). Indeed, they violate Neumann's principle that the macroscopic properties of a perfect crystal must have at least the point-group symmetry of that crystal (34, 35). In Fig. 1 *C* and *E*, we show the ARTR data taken from a $Sr_2RuO_4$/LSAT sample at temperatures $T = 295$ K and $T = 4$ K, respectively. In both cases, and at every temperature in between, $\rho_T(\phi)$ oscillates with the period of 180° in $\phi$, with the sign alternating between positive and negative. All of the experimental data of $\rho_T(\phi)$ (solid dots) can be well fit (the solid red curves in Fig. 1 *C* and *E*) by the simple expression **[2]** with only two free parameters, the amplitude $\rho_T{}^0$ and the phase offset $\alpha$. In Fig. 1 *D* and *F*, we show the corresponding $\rho(\phi)$ data (blue solid dots). The red dashed curves are not independent fits to these $\rho(\phi)$ data; rather, they are calculated using as an input the values of $\rho_T{}^0$ and $\alpha$ inferred from the $\rho_T(\phi)$ data, shifted up by the angle-averaged longitudinal resistivity $\bar{\rho}$ and then left by 45°. Apparently, the angular oscillations in $\rho(\phi)$ and $\rho_T(\phi)$ have the same amplitude and are phase-shifted exactly as predicted by Eqs. **1** and **2**. This is an unambiguous manifestation of anisotropy in the electric transport in the *a*-*b* plane of the $Sr_2RuO_4$ film.

To make this more intuitive, in Fig. 1 *G* and *H* we plot the same data as in Fig. 1 *E* and *F*, respectively, but in polar coordinates, where the radial distance scales with the $\rho_T(\phi)$ and $\rho(\phi)$ data measured at $T = 4$ K. The patterns show that the symmetry in the electronic transport is $\mathbf{C}_2$, reduced compared to the $\mathbf{C}_4$ symmetry of the lattice. The "cloverleaf" shape in $\rho_T(\phi)$ should not be confused with the *d*-wave gap symmetry in the momentum space; this is just a consequence of the existence of easy and hard transport axes in real space. This is corroborated by the "peanut" shape in $\rho(\phi)$, as seen in Fig. 1*H*.

Comparing the data at $T = 4$ K and $T = 295$ K, it is apparent that $\rho_T{}^0$ varies with $T$ substantially. In contrast, $\alpha$ remains roughly the same: $\alpha = 68°$ at $T = 4$ K and $\alpha = 65°$ at $T = 295$ K. Hence,

the principal axes of the resistivity tensor are fixed in real space regardless of the sample temperature. It is visually clear in Fig. 1 *G* and *H* that the angles at which the values of $\rho_T(\phi)$ or $\rho(\phi)$ peak do not coincide with the crystallographic axes of the $Sr_2RuO_4$ or the underlying substrate. The fact that the principal axes do not align with the crystallographic axes defies Neumann's principle (34, 35) and rules out the possibility that the observed "nematicity" simply originates in the anisotropy of the $Sr_2RuO_4$ lattice imposed by epitaxy on a substrate with a twofold rather than a fourfold symmetry axis perpendicular to it.

We have made extensive efforts to minimize the angular oscillations in $\rho_T(\phi)$ and $\rho(\phi)$ that are caused by extrinsic factors, e.g., contact misalignment, film inhomogeneity and imperfections, film thickness variations, etc. In addition to detailed and targeted experiments already performed (15), we have fabricated a sunbeam device out of a conventional metal (Ti), using the same lithography mask and process to further address the concerns about the lithography process and measurement setup. The ARTR measurements on this control sample indeed show the absence of any angular oscillations in $\rho_T(\phi)$ and $\rho(\phi)$ (see *SI Appendix* for details). This clearly shows that the observed angular oscillations must originate from $Sr_2RuO_4$. On the other hand, the symmetry of the observed patterns (Figs. 1*H* and 2*F*) and the large magnitude of the observed effect eliminate the possibility that they might originate from conceivable small gradients in the film composition or thickness.

To further explore the effects of lattice distortions, for comparison we have also studied $Sr_2RuO_4$ films epitaxially grown on (110) $NdGaO_3$, a deliberately chosen orthorhombic substrate. The films were thin enough (23 nm) that the $Sr_2RuO_4$ lattice in this case is forced to be orthorhombic by the commensurate epitaxial strain. The X-ray diffraction experiments, on the same samples on which $\rho_T(\phi)$ and $\rho(\phi)$ were measured, confirmed this expectation (see *SI Appendix* for details). The *a* and *b* lattice constants differ by 0.5% in the $NdGaO_3$ substrate as well as in the $Sr_2RuO_4$ films grown upon it. In contrast, in the $Sr_2RuO_4$ film on LSAT the difference is just 0.03%, more than one order of magnitude smaller. ARTR measurements on $Sr_2RuO_4$/$NdGaO_3$ films also revealed strong angular oscillations with a period of 180° in both $\rho_T(\phi)$ and $\rho(\phi)$ at $T = 4$ K as well as at $T =$ 295 K (Fig. 2 *A*–*D*). Like in the $Sr_2RuO_4$/LSAT sample, these $\rho_T(\phi)$ and $\rho(\phi)$ oscillations can be simultaneously well fit by Eqs. **1** and **2** at a given temperature. The fits yield $\alpha = 7^\circ$ at $T = 4$ K and $\alpha = 6°$ at $T = 295$ K. The plots in polar coordinates (Fig. 2 *D* and *F*) show this more intuitively: the in-plane directions corresponding to $\rho_{max}$ and $\rho_{min}$ are nearly parallel to the $Sr_2RuO_4$/$NdGaO_3$ crystallographic [100] and [001] directions of $Sr_2RuO_4$, respectively. Note, however, that we have repeated the growth of $Sr_2RuO_4$ on (110) $NdGaO_3$ substrates multiple times and found that in some samples the principal axes are not aligned with either of the crystallographic directions (see *SI Appendix* for details). This indicates that the orthorhombic distortion induced in the $Sr_2RuO_4$ lattice by the epitaxial strain from $NdGaO_3$ is barely at the border of being strong enough to pin the orientation of nematicity in the electron fluid.

Turning the focus on the amplitude of nematic order, we explore how it depends on temperature and on the epitaxially imposed lattice distortion. To facilitate a quantitative comparison, we define the magnitude of the nematicity as $N = \rho_T^0/\overline{\rho}$. In analogy to the Hall angle, *N* has a geometric interpretation; it is equal to the arctangent of the angle between the directions of the electric field and current-density vectors. Thus, *N* is an intrinsic quantity characteristic of every nematic material. We measured *N* continuously as a function of temperature. In both $Sr_2RuO_4$/LSAT and $Sr_2RuO_4$/$NdGaO_3$, $N(T)$ increases rapidly as *T* decreases (Fig. 3), implying that the nematic order is strengthened

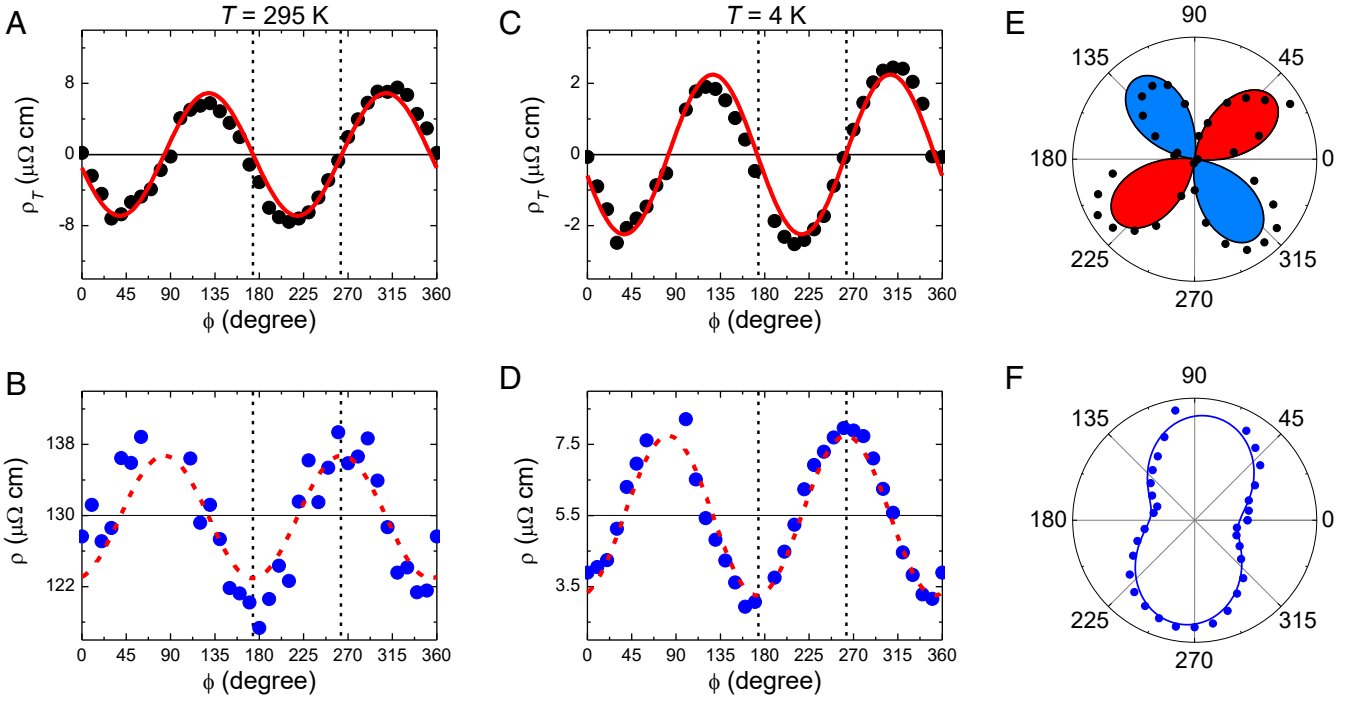


**Fig. 2.** $\rho_T(\phi)$ and $\rho(\phi)$ of an orthorhombic $Sr_2RuO_4$ film on a (110) $NdGaO_3$ substrate. In ultrathin $Sr_2RuO_4$ films grown on orthorhombic (110) $NdGaO_3$ substrates, the difference between *a* and *b* lattice constants is 0.5%, an order of magnitude larger than in $Sr_2RuO_4$ films on LSAT. (*A*) The $\rho_T(\phi)$ data (black dots) measured at $T = 295$ K and the fit (solid red curve) to $\rho_T(\phi) = \rho_T{}^0\sin[2(\phi-\alpha)]$, with $\alpha = -6°$. The black dashed lines are defined the same way as in Fig. 1. (*B*) The $\rho(\phi)$ data (blue dots) measured at $T = 295$ K are well reproduced (the dashed red line) by the curve obtained by fitting $\rho_T(\phi)$, and shifted upward by a constant, $\overline{\rho}$, and left by 45°. (*C*) The same as in *A* but for $T = 4$ K. (*D*) The same as in *B* but for $T = 4$ K. (*E*) The same as in *C* but plotted in polar coordinates; the experimental data (black dots) and the fit curve (the solid line). Blue filling indicates positive and red negative values. (*F*) The same as in *D*, in polar coordinates.

as the thermal fluctuations diminish. Next, one can see that $N$ is nearly equal in $Sr_2RuO_4$/LSAT and $Sr_2RuO_4$/$NdGaO_3$ at every temperature, despite more than an order of magnitude difference between the lattice distortions. If the origin of nematicity were in the anisotropy of the lattice, or of the electron–lattice coupling, $N$ should have increased fast with the lattice distortion, in variance with the experimental observations.

The corresponding temperature-dependent $\rho_T(T)$ and $\rho(T)$, measured at three representative directions, are shown in *SI Appendix*. As the temperature is increased, both $\rho_T(T)$ and $\rho(T)$ increase monotonically. In contrast, $N(T)$ decreases, and one could indeed surmise that it should vanish at some temperature $T^*$. Unfortunately, this $T^*$ cannot be measured directly since $Sr_2RuO_4$ films lose oxygen and decompose at elevated temperatures. Nevertheless, it is clear that $N(T)$ deviates significantly from the mean-field–like $(T^*-T)^{1/2}$ dependence; the shape of $N(T)$ is concave instead of convex. Note that the same behavior is seen in $La_{2-x}Sr_xCuO_4$ (15) in $N(T)$ as well as in other key physical parameters such as the upper critical magnetic field $H_{c2}$, etc., which has been ascribed to the presence of strong fluctuations over a broad $T$ range.

The next important question is how is nematicity related to superconductivity, and more specifically, whether the nematic amplitude traverses through the superconducting transition smoothly or with some jump or kink at $T_c$. We have addressed this question in three ways. One is that in $Sr_2RuO_4$ superconductivity is sensitive to uniaxial strain (23). Our $Sr_2RuO_4$ films are under biaxial strain imposed by the underlying substrate. Although less established, we do observe biaxial strain to affect superconductivity in addition to the other factors described below. The $Sr_2RuO_4$/LSAT film studied in Fig. 1 is metallic but not superconducting, at least down to $T = 300$ mK, the lowest temperatures available in our Helium-3 cryogenic setup. In contrast, the $Sr_2RuO_4$/$NdGaO_3$ film studied in Fig. 2 has $T_c \sim 0.9$ K, as shown in *SI Appendix*. Nevertheless, the amplitudes of nematicity are substantial and nearly equal in $Sr_2RuO_4$/LSAT and $Sr_2RuO_4$/$NdGaO_3$ (Fig. 3). The other testing opportunity stems from the fact that unlike the superconductivity in conventional metals, the superconductivity in $Sr_2RuO_4$ is very sensitive to even a minor amount of chemical impurities and other structural imperfections. It was reported that as the residual resistivity of $Sr_2RuO_4$ increases, $T_c$ decreases sharply to zero (22). Precisely for this reason, it has been an extremely challenging task to synthesize superconducting $Sr_2RuO_4$ films. Indeed, $Sr_2RuO_4$ films with the growth conditions even slightly off the optimal growth recipe turn out not to be superconducting. We have thus been able to study, for comparison, an $Sr_2RuO_4$/$NdGaO_3$ film that has an essentially identical lattice structure and a similar longitudinal resistivity at room temperature as the superconducting film in Fig. 2, but has a somewhat larger residual resistivity and is not superconducting down to $T = 0.3$ K. ARTR measurement on this sample showed $\rho_T(\phi)$ and $\rho(\phi)$ nearly identical to those shown in Fig. 2 (see *SI Appendix* for details) regardless of the differences in disorder and superconductivity. The third way is to suppress the superconductivity by an external magnetic field and show that this underlying metallic state is also nematic, with both $N(T)$ and $\alpha(T)$ seamlessly connecting to their zero-field dependences above $T_c$. Altogether, the above shows that the nematic state of $Sr_2RuO_4$ is intrinsic and more robust than superconductivity.

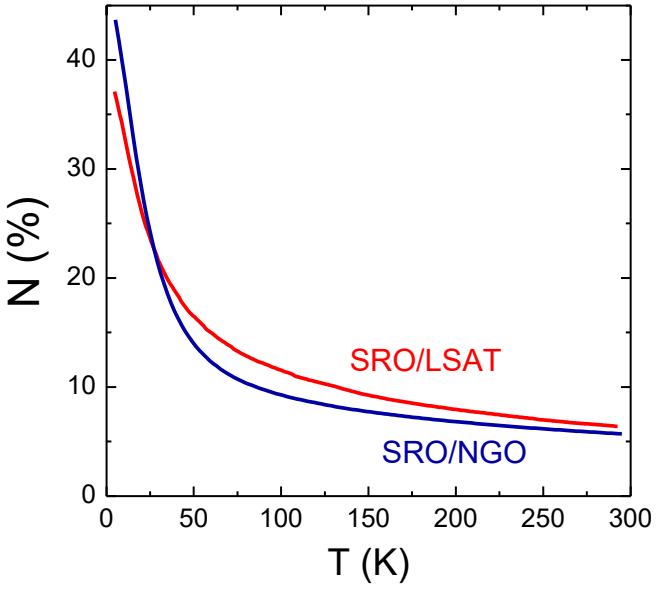


**Fig. 3.** Temperature dependence of the nematicity magnitude $N$ in the $Sr_2RuO_4$/LSAT and $Sr_2RuO_4$/$NdGaO_3$ samples. In analogy to the Hall angle, the magnitude of nematicity is defined as $N = \rho_T^0/\bar{\rho}$. It increases as $T$ decreases in both samples. At any temperature below 300 K, the values of $N$ in $Sr_2RuO_4$/LSAT and $Sr_2RuO_4$/$NdGaO_3$ are close to one another, despite the fact that the orthorhombic distortion is more than an order of magnitude larger (0.5%) in $Sr_2RuO_4$/$NdGaO_3$ than in $Sr_2RuO_4$/LSAT (0.03%). Apparently, the lattice distortion only affects the principal axes (i.e., the orientation of nematicity) but has almost no effect on the magnitude of the nematicity.

Having established that the resistivity tensor of $Sr_2RuO_4$ appears to break Neumann's principle based on the established symmetry of $Sr_2RuO_4$ and the substrates upon which we grew commensurate $Sr_2RuO_4$ films, we now turn to the question of why? The definite answer would require a quantitative theoretical analysis that is beyond the scope of the present experimental paper, but we can offer some general reflections.

One possibility is that the true symmetry of $Sr_2RuO_4$ is not tetragonal and that a small distortion exists in it that has not been detected by all prior structural studies. In the structurally related compound, $Sr_3Ru_2O_7$, a structural distortion $\varepsilon = (a - b)/(a + b) \sim 10^{-7}$ that breaks the fourfold symmetry axis below 1.2 K in magnetic fields of 8 T has been detected (36). Such a tiny structural distortion would be below the resolution $\varepsilon \sim 10^{-4}$ of the X-ray techniques used to establish the structure of $Sr_2RuO_4$ (33). But, for such a small distortion to cause the large anisotropy in transport that we see, the nematic susceptibility, $dN/d\varepsilon$, would have to be very large in $Sr_2RuO_4$. If that were the case, perhaps some symmetry-breaking defects in $Sr_2RuO_4$—e.g., such that could arise from step edges that accompany the slight misorientation of the substrates from precisely (001) LSAT and precisely (110) $NdGaO_3$—could lead to a substantial transverse voltage. As described in *SI Appendix*, the substrates used in this study are all oriented within ±0.2°. This together with the extreme sensitivity of superconductivity in $Sr_2RuO_4$ to disorder implies that the defect concentration of these $Sr_2RuO_4$ films is small. For standard materials, such minor symmetry breaking from defects would have an imperceptible effect on the measured properties. With a sufficiently large nematic susceptibility, however, this situation can change.

The main problem with the above scenario is that if the nematic susceptibility were very large, one would indeed expect $N$ to grow fast with $\varepsilon$, contrary to what we see—$N$ is nearly the same in $Sr_2RuO_4$ grown on tetragonal LSAT and orthorhombic NGO substrates, i.e., it seems almost independent of $\varepsilon$.[§]

A more likely option is that for very small $\varepsilon$, $dN/d\varepsilon$ is indeed very large and sufficient to propel the system into a state with a

[§]The same is true in $La_{2-x}Sr_xCuO_4$, as well (15).

substantial transport anisotropy, but once that state is reached, $dN/d\varepsilon$ gets small. Think of a system in a double-well potential, being in unstable equilibrium if it is in the high-symmetry configuration. In this scenario, $Sr_2RuO_4$ is an electronic nematic over the entire range of our measurements (300 to 4 K). As the temperature is reduced, superconductivity emerges out of the nematic normal state. As for the superconducting state, we have no direct information, since the ARTR technique is "blinded" once the resistance drops to zero, but one can state what seems plausible. The spontaneous breaking of the rotational symmetry in the normal state, as reported here in $Sr_2RuO_4$, probably indicates that the electron–electron interaction is anisotropic in the *a-b* plane. If that is the case, the rotationally-symmetric *s*-wave superconducting state may be energetically less favorable. Rather, one would expect the strength of Cooper pairing to oscillate with the azimuth angle $\phi$, giving rise to a superconducting state with nodes and antinodes along different orientations, like in cuprates.

The experimental status of the symmetry of the superconducting order parameter in $Sr_2RuO_4$ seems unclear. For many years, $Sr_2RuO_4$ has been considered as a candidate for *p* wave or more generally for spin-triplet superconductivity (24–28). A recent NMR experiment, however, indicated that the superconducting order parameter of the superconducting state of $Sr_2RuO_4$ is not odd parity (29), hence, not *p* wave. The results presented here indicate that the *s*-wave state is also unlikely. Taken together, this narrows the options down, and may help resolve this important question.

Yet another option is that in $Sr_2RuO_4$ there are significant intracell atomic displacements of oxygen ions that break the $\mathbf{C_4}$ symmetry but without affecting the lattice constants. These would be difficult to detect by standard X-ray diffraction techniques, additionally abated by the weak X-ray scattering on oxygen. Then any small external field could favor one direction over the other, and the long-range nature of the Madelung energy could make the single-orientation domains large and/or their distribution strongly imbalanced; this must be the case since we observe anisotropy in transport in our ARTR measurements that probe the sample on the mm scale.

Thus, the present work motivates experiments aimed at resolving among the options listed. One direction would be to study the nematic susceptibility by elastoresistivity measurements (37, 38). If the measurements can be extended down to the 10 mK scale (in a dilution refrigerator), one may even be able to resolve whether $dN/d\varepsilon$ diverges when $T \to T_c$ or when $T \to 0$, if at all; such data would provide critical input to theory, including the exciting proposal that in $Sr_2RuO_4$ superconductivity may be driven, or enhanced by nematic fluctuations (39, 40). Another, technically challenging but potentially quite illuminating study, would be to directly measure the intracell oxygen displacements in $Sr_2RuO_4$, if any.

In summary, we believe that the ARTR data reported here in $Sr_2RuO_4$, and previously in copper-oxide superconductors (15), indicate that the unconventional superconductivity and the nematicity (or a large nematic susceptibility) may be both ascribed to strong and anisotropic electron correlations. We conjecture that electronic nematicity may be widespread in strongly correlated materials, and our ARTR technique provides a direct and simple way for its detection and characterization.

**Data and Materials Availability.** Data needed to evaluate the conclusions of this manuscript are presented in the main text and *SI Appendix*.

**ACKNOWLEDGMENTS.** We thank A. Mackenzie and A. Gozar for valuable discussions. The research at Brookhaven National Laboratory was supported by the US Department of Energy, Basic Energy Sciences, Materials Sciences and Engineering Division. X.H. is supported by the Gordon and Betty Moore Foundation's EPiQS Initiative Grant GBMF9074. H.P.N., N.J.S., K.M.S., and D.G.S. acknowledge support from the National Science Foundation (Platform for the Accelerated Realization, Analysis and Discovery of Interface Materials) under Cooperative Agreement DMR-1539918 and from the W.M. Keck Foundation. N.J.S. acknowledges support from the National Science Foundation Graduate Research Fellowship Program under Grant DGE-1650441. This publication is funded in part by the Gordon and Betty Moore Foundation through Grant GBMF9073 to Cornell University. Substrate preparation was performed in part at the Cornell NanoScale Facility, a member of the National Nanotechnology Coordinated Infrastructure, which is supported by the NSF (Grant ECCS-1542081).

1. S. A. Kivelson, E. Fradkin, V. J. Emery, Electronic liquid-crystal phases of a doped Mott insulator. *Nature* **393**, 550–553 (1998).
2. V. Oganesyan, S. A. Kivelson, E. Fradkin, Quantum theory of a nematic Fermi fluid. *Phys. Rev. B Condens. Matter Mater. Phys.* **64**, 195109 (2001).
3. E. Fradkin, S. A. Kivelson, M. J. Lawler, J. P. Eisenstein, A. P. Mackenzie, Nematic Fermi fluids in condensed matter physics. *Ann. Rev. Cond. Mat. Phys.* **1**, 153–178 (2010).
4. E. W. Carlson, K. A. Dahmen, Using disorder to detect locally ordered electron nematics via hysteresis. *Nat. Commun.* **2**, 379 (2011).
5. B. Phillabaum, E. W. Carlson, K. A. Dahmen, Spatial complexity due to bulk electronic nematicity in a superconducting underdoped cuprate. *Nat. Commun.* **3**, 915 (2012).
6. Y. Ando, K. Segawa, S. Komiya, A. N. Lavrov, Electrical resistivity anisotropy from self-organized one dimensionality in high-temperature superconductors. *Phys. Rev. Lett.* **88**, 137005 (2002).
7. V. Hinkov *et al*., Electronic liquid crystal state in the high-temperature superconductor $YBa_2Cu_3O_{6.45}$. *Science* **319**, 597–600 (2008).
8. M. J. Lawler *et al*., Intra-unit-cell electronic nematicity of the high-$T_c$ copper-oxide pseudogap states. *Nature* **466**, 347–351 (2010).
9. R. Daou *et al*., Broken rotational symmetry in the pseudogap phase of a high-$T_c$ superconductor. *Nature* **463**, 519–522 (2010).
10. K. Fujita *et al*., Simultaneous transitions in cuprate momentum-space topology and electronic symmetry breaking. *Science* **344**, 612–616 (2014).
11. Y. Lubashevsky, L. Pan, T. Kirzhner, G. Koren, N. P. Armitage, Optical birefringence and dichroism of cuprate superconductors in the THz regime. *Phys. Rev. Lett.* **112**, 147001 (2014).
12. O. Cyr-Choinière *et al*., Two types of nematicity in the phase diagram of the cuprate superconductor $YBa_2Cu_3O_y$. *Phys. Rev. B Condens. Matter Mater. Phys.* **92**, 224502 (2015).
13. J. Zhang *et al*., Anomalous thermal diffusivity in underdoped $YBa_2Cu_3O_{6+x}$. *Proc. Natl. Acad. Sci. U.S.A.* **114**, 5378–5383 (2017).
14. Y. Sato *et al*., Thermodynamic evidence for a nematic phase transition at the onset of the pseudogap in $YBa_2Cu_3Oy$. *Nat. Phys.* **13**, 1074–1078 (2017).
15. J. Wu, A. T. Bollinger, X. He, I. Božović, Spontaneous breaking of rotational symmetry in copper oxide superconductors. *Nature* **547**, 432–435 (2017).
16. J.-H. Chu *et al*., In-plane resistivity anisotropy in an underdoped iron arsenide superconductor. *Science* **329**, 824–826 (2010).
17. T.-M. Chuang *et al*., Nematic electronic structure in the "parent" state of the iron-based superconductor $Ca(Fe_{(1-x)}Co_{(x)})_2As_2$. *Science* **327**, 181–184 (2010).
18. R. M. Fernandes, A. V. Chubukov, J. Schmalian, What drives nematic order in iron-based superconductors? *Nat. Phys.* **10**, 97–104 (2014).
19. S. Kasahara *et al*., Electronic nematicity above the structural and superconducting transition in $BaFe_2(As_{(1-x)}P_{(x)})_2$. *Nature* **486**, 382–385 (2012).
20. F. Ronning *et al*., Electronic in-plane symmetry breaking at field-tuned quantum criticality in $CeRhIn_5$. *Nature* **548**, 313–317 (2017).
21. C. M. Varma, L. Zhu, Helicity order: Hidden order parameter in $URu_2Si_2$. *Phys. Rev. Lett.* **96**, 036405 (2006).
22. A. P. Mackenzie *et al*., Extremely strong dependence of superconductivity on disorder in $Sr_2RuO_4$. *Phys. Rev. Lett.* **80**, 161–164 (1998).
23. A. Steppke *et al*., Strong peak in $T_c$ of $Sr_2RuO_4$ under uniaxial pressure. *Science* **355**, 148 (2017).
24. T. M. Rice, M. Sigrist, $Sr_2RuO_4$: An electronic analogue of $^3$He? *J. Phys. Condens. Matter* **7**, L643–L648 (1995).
25. Y. Maeno *et al*., Superconductivity in a layered perovskite without copper. *Nature* **372**, 532–524 (1994).
26. A. P. Mackenzie, Y. Maeno, The superconductivity of $Sr_2RuO_4$ and the physics of spin-triplet pairing. *Rev. Mod. Phys.* **75**, 657–712 (2003).
27. Y. Maeno, S. Kittaka, T. Nomura, S. Yonezawa, K. Ishida, Evaluation of spin-triplet superconductivity in $Sr_2RuO_4$. *J. Phys. Soc. Jpn.* **81**, 1–29 (2012).
28. A. P. Mackenzie, T. Scaffidi, C. W. Hicks, Y. Maeno, Even odder after twenty-three years: The superconducting order parameter puzzle of $Sr_2RuO_4$. *Npj Quantum Mater.* **2**, 40 (2017).
29. A. Pustogow *et al*., Constraints on the superconducting order parameter in $Sr_2RuO_4$ from oxygen-17 nuclear magnetic resonance. *Nature* **574**, 72–75 (2019).
30. H. P. Nair *et al*., Demystifying the growth of superconducting $Sr_2RuO_4$ thin films. *APL Mater.* **6**, 101108 (2018).

31. M. Steins, J. Doerschel, P. Reiche, Crystal structure of aluminium lanthanum strontium tantalum oxide, $(La_{0.272}Sr_{0.728})(Al_{0.648}Ta_{0.352})O_3$. *Z. Kristallogr. New Cryst. Struct.* **212**, 77 (1997).
32. L. J. van der Pauw, A method of measuring specific resistivity and Hall effect of discs of arbitrary shape. *Philips Res. Rep.* **20**, 220–224 (1958).
33. L. Walz, F. Lichtenberg, Refinement of the structure of $Sr_2RuO_4$ with 100 and 295 K X-ray data. *Acta Crystallogr. C* **49**, 1268–1270 (1993).
34. W. Voigt, *Lehrbuch der Kristallphysik* (Teubner, Leipzig, 1910), pp. 3–23.
35. J. F. Nye, *Physical Properties of Crystals: Their Representation by Tensors and Matrices* (Oxford University Press, 1985) pp. 20–24.
36. C. Stingl, R. S. Perry, Y. Maeno, P. Gegenwart, Symmetry-breaking lattice distortion in $Sr_3Ru_2O_7$. *Phys. Rev. Lett.* **107**, 026404 (2011).
37. J.-H. Chu, H.-H. Kuo, J. G. Analytis, I. R. Fisher, Divergent nematic susceptibility in an iron arsenide superconductor. *Science* **337**, 710–712 (2012).
38. H.-H. Kuo, J.-H. Chu, J. C. Palmstrom, S. A. Kivelson, I. R. Fisher, Ubiquitous signatures of nematic quantum criticality in optimally doped Fe-based superconductors. *Science* **352**, 958–962 (2016).
39. S. Lederer, Y. Schattner, E. Berg, S. A. Kivelson, Enhancement of superconductivity near a nematic quantum critical point. *Phys. Rev. Lett.* **114**, 097001 (2015).
40. R. M. Fernandes, S. A. Kivelson, E. Berg, Vestigial chiral and charge orders from bidirectional spin-density waves: Application to the iron-based superconductors. *Phys. Rev. B* **93**, 014511 (2016).

# Supplementary Materials for

## Title: Electronic nematicity in $Sr_2RuO_4$

J. Wu[1,*], H. P. Nair[2,*], A. T. Bollinger[1], X. He[1,3], I. Robinson[1], N. J. Schreiber[2], K. M. Shen[4,5], D. G. Schlom[2,5], and I. Božović[1,3]

Correspondence to: bozovic@bnl.gov

**This PDF file includes:**

Materials and Methods
Supplementary Text
Figs. SF1 to SF5
Tables ST1 to ST3
Supplementary references *(SR1)-(SR10)*



www.pnas.org/cgi/doi/10.1073/pnas.1921713117

## Materials and Methods

### Materials

High-quality single crystal films of (001)-oriented $Sr_2RuO_4$ were synthesized in a Veeco GEN10 molecular-beam epitaxy system. Well-oriented 10 mm × 10 mm × 1 mm single-crystal substrates of (110) $NdGaO_3$ and (001) $(LaAlO_3)_{0.29}$–$(Sr_{1/2}Al_{1/2}TaO_3)_{0.71}$ (LSAT) from CrysTec GmbH *(31)* were heated to growth temperatures in the range 870 °C to 910 °C, as measured by an optical pyrometer operating at 1,550 nm. There they were exposed to molecular beams of strontium (99.99% purity), ruthenium (99.99% purity), and distilled ozone (~80% $O_3$ + 20% $O_2$ made from oxygen gas with 99.994% purity), all supplied at the same time (co-deposition). The strontium and ruthenium fluxes ranged from about $1.9\times10^{13}$ to $3.3\times10^{13}$ atoms·cm$^{-2}$s$^{-1}$ and $1.4\times10^{13}$ to $2.5\times10^{13}$ atoms·cm$^{-2}$s$^{-1}$, respectively, corresponding to an excess ruthenium flux of about $2\times10^{12}$ to $9\times10^{12}$ atoms·cm$^{-2}$s$^{-1}$ for the growth of $Sr_2RuO_4$. The growth rate of the $Sr_2RuO_4$ films ranged from 0.09 Å/s to 0.16 Å/s. To facilitate radiative coupling between the SiC substrate heater filament and the substrates, the back sides of the substrates were coated with a 10 nm thick titanium adhesion layer followed by 400 nm of platinum followed by 200 nm of polycrystalline $SrRuO_3$. The background oxidant pressure during growth ranged from of $8\times10^{-7}$ Torr to $1\times10^{-6}$ Torr. At the completion of growth, the strontium and ruthenium shutters were simultaneously closed, and the film was rapidly cooled to below 250 °C in the same pressure of distilled ozone in which it was grown. Strontium was evaporated from a low-temperature cell while an electron-beam evaporator was used for ruthenium. A typical X-ray diffraction pattern is shown in Fig. SF1, and Reflection high-energy electron diffraction (RHEED) pattern in Fig. SF2.Additional details, including the growth window for the adsorption-controlled conditions used, may be found elsewhere *(SR1)*.

The best of our $Sr_2RuO_4$ films are superconducting with the critical temperature $T_c \approx 1.5$ K, as high as in the best bulk $Sr_2RuO_4$ crystals *(SR1)*.

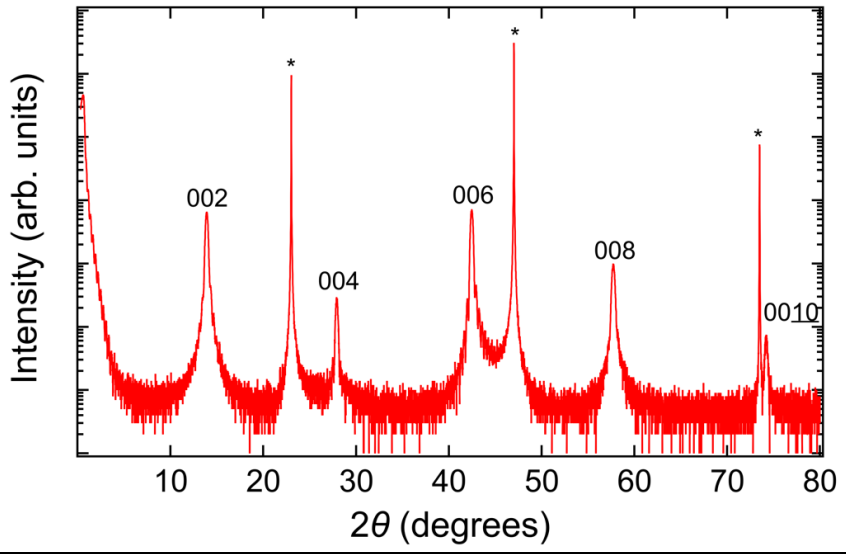


**Fig. SF1. X-ray diffraction $\theta$-$2\theta$ scan of a ~30 nm thick (001)-oriented $Sr_2RuO_4$ film grown on a $NdGaO_3$(110) substrate.** All of the peaks in the scan can be indexed to either the film or the substrate (asterisks).

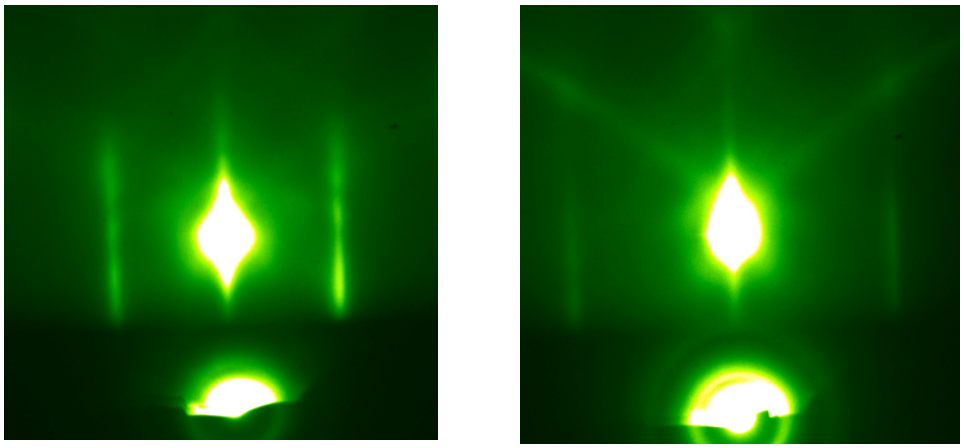

**Fig. SF2. Reflection high-energy electron diffraction (RHEED) from the same film.** **a,** The RHEED pattern recorded with the electron beam incident along the <100> azimuth of the $Sr_2RuO_4$ thin film. **b,** the same, but with the beam incident along the <110> azimuth. The RHEED patterns were recorded at a substrate temperature of 300 ˚C at the end of the growth.

## Methods

The $Sr_2RuO_4$ films were patterned by standard photo-lithography procedures to form the "sun-beam" pattern shown in Fig. 1a in the main text. The precision in the alignment of lithography is ±1 μm. The electric current runs along a chosen Hall bar at a time with the corresponding longitudinal or transverse voltages being recorded using three pairs of evenly-spaced gold contacts (Fig. 1b) on the Hall bar. The angle $\Delta\phi$ between two successive Hall bars is $10^0$ and the total of 36 Hall bars systematically map out the in-plane angle $\phi$ from $0^0$ to $350^0$. The orientation of the Hall bar with the initial angle $\phi = 0^0$ is aligned with the [100] crystal axis of $Sr_2RuO_4$ with a precision of $0.1^0$.

The transport measurements were carried out in both Helium-4 and Helium-3 cryogenics to study the temperature dependence of longitudinal and transverse resistivity. The thermal stability of both systems is better than ±1 mK.

# Supplementary Text

## 1. Lattice orthorhombicity determined by XRD

Single crystal X-ray diffraction was used to determine the lattice constants of the $Sr_2RuO_4$ films on the two substrates, $NdGaO_3$ and LSAT. An in-house Bruker D8 4-circle diffractometer was used to locate the angular positions of a number of peaks from the films using $\lambda$ = 1.540 Å, 0.5 mm resolution-defining slits and a 1 mm out-of-plane detector slit to provide 3D resolution. Following the standard angle convention of Busing and Levy (*SR2)*, for each reflection the detector angle ($2\theta$), the sample angle ($\theta$) and the tilt Euler angle ($\chi$) were scanned in sequence until consistent, while the azimuthal Euler angle ($\phi$) was kept fixed. The peak center positions of seven accessible reflections were least-squares-fit to a general lattice without constraints to determine the lattice constants (*SR3*). The self-consistency of the fit was used to generate an absolute error, the distance in reciprocal space between the reciprocal lattice point and its measured position. These errors were then used as a conservative estimate of the accuracy of the measured lattice constants.

Tables ST1 and ST2 show the measured angles and the resulting errors for the least-squares fit. It is clear that the errors are well distributed and at the level expected for a slit-defined instrument. Table ST1 shows the measured lattice parameters of $Sr_2RuO_4$ films grown on LSAT substrate. The LSAT is less precisely measured, but consistent with $a = b$, or a tetragonal structure of the film. Table ST2 shows the measured lattice parameters of $Sr_2RuO_4$ films grown on $NdGaO_3$ substrate. The measured values of $a$ and $b$ for $Sr_2RuO_4$ on $NdGaO_3$ are no longer consistent with $a = b$, so we conclude this film to be orthorhombic.

| H | K | L | 2 $\theta$ | $\theta$ | $\varphi$ | $\chi$ | Error (Å$^{-1}$) |
|---|---|---|---|---|---|---|---|
| **1** | -1 | 4 | 43.50 | 21.760 | -46.26 | 40.61 | 0.0039 |
| **-1** | 1 | 4 | 43.50 | 21.761 | 133.51 | 40.64 | 0.0039 |
| **-1** | -1 | 4 | 43.51 | 21.770 | 223.52 | 40.76 | 0.0025 |
| **1** | 1 | 4 | 43.53 | 21.766 | 43.71 | 40.50 | 0.0047 |
| **0** | 1 | 3 | 31.23 | 15.619 | 88.60 | 42.46 | 0.0067 |
| **-1** | 0 | 3 | 31.23 | 15.622 | 178.45 | 42.53 | 0.0045 |
| **1** | 0 | 3 | 31.23 | 15.619 | -1.21 | 42.41 | 0.0055 |

**Table ST1**. The measured diffractometer angles and the resulting errors to the least-squares fit for $Sr_2RuO_4$ films on LSAT.

| H | K | L | 2 $\theta$ | $\theta$ | $\varphi$ | $\chi$ | Error (Å$^{-1}$) |
|---|---|---|---|---|---|---|---|
| **-1** | 0 | 3 | 31.31 | 15.566 | 225.50 | 42.11 | 0.0020 |
| **0** | 1 | 3 | 31.22 | 15.607 | 135.51 | 42.12 | 0.0030 |
| **1** | 0 | 3 | 31.31 | 15.649 | 45.65 | 42.05 | 0.0025 |
| **0** | -1 | 3 | 31.26 | 15.614 | -44.44 | 42.36 | 0.0036 |

| | | | | | | | |
|---|---|---|---|---|---|---|---|
| **1** | 1 | 4 | 43.55 | 21.787 | 90.50 | 40.37 | 0.0021 |
| **-1** | 1 | 4 | 43.58 | 21.771 | 180.46 | 40.34 | 0.0037 |
| **1** | -1 | 4 | 43.56 | 21.787 | 0.73 | 40.45 | 0.0038 |

**Table ST2**. The measured diffractometer angles and the resulting errors to the least-squares fit for $Sr_2RuO_4$ films on $NdGaO_3$.

| Substrate | a | b | c | α | β | γ | Volume (Å$^3$) |
|---|---|---|---|---|---|---|---|
| **LSAT** | 3.873(11) | 3.874(11) | 12.75(4) | 90.09 | 89.98 | 90.01 | 190 |
| **$NdGaO_3$** | 3.848(7) | 3.861(7) | 12.79(2) | 90.00 | 89.99 | 89.95 | 191 |

**Table ST3**. Measured lattice parameters of $Sr_2RuO_4$ films on the two different substrates. Errors estimated from the misfit of the lattice are shown in parentheses.

## 2. Pitfalls of using the van der Pauw method to probe nematicity

The van der Pauw method is commonly used to measure the resistivity of single crystals. This method, as it was originally conceived and most widely utilized (*SR4*) is appropriate for measuring the resistivity of materials with isotropic in-plane conductivity. For materials with anisotropic resistivity, e.g., when it is desired to probe for electronic nematicity, this approach has pitfalls of which one should be aware (*SR5,SR6*). Below is an example that illustrates the subtlety.

On a uniform as-grown $Sr_2RuO_4$ film on an (110) $NdGaO_3$ substrate, four point contacts were wire-bonded onto the four corners to carry out the van der Pauw measurements. The recorded $R(T)$ along two orthogonal directions [001] and $[1\bar{1}0]$ manifest significant difference (Fig. SF3a), confirming $R_a \neq R_b$ and consequently the nematicity. Intuitively, one would expect that the magnitude of the nematicity $N$ should be proportional to $\Delta R$ ($= R_a - R_b$). If that were true, $N$ should first decrease with sample cooling until it vanishes at $T \sim 40$ K, and on further cooling $N$ should increase, but with the opposite sign. This inferred peculiar $N(T)$ behavior is, however, merely an artifact due to misinterpretation of the van der Pauw method. To illustrate this, we patterned the same $Sr_2RuO_4$ film with the sun-beam lithography pattern (Fig. 1a) and measured the longitudinal resistivity $\rho$ along the same [001] and $[1\bar{1}0]$ directions. One can see that $\rho_a \neq \rho_b$, i.e., the electronic state is nematic, consistent with Fig. SF3a. Remarkably, the $\rho_a(T)$ and $\rho_b$ $T$) do not cross at any $T$ from 295 K down to 4 K (Fig. SF3b). The calculated $N(T)$ does not change sign at any temperature; it monotonically increases as $T$ decreases, similar to $N(T)$ shown in Fig. 3.

The merit of the sun-beam method is that the excitation current is guided by the Hall bar geometry to run uniformly along a given direction (*SR7*). Conversely, in the van der Pauw method, the current density $\boldsymbol{j}$ between two current contacts varies locally in both direction and amplitude. More importantly, the spatial distribution of $\boldsymbol{j}$ is susceptible to the magnitude of the nematicity. Thus, the correct interpretation of the measured $R_a$ and $R_b$ demands a delicate self-consistent modeling of $\boldsymbol{j}$ under the influence of the unknown $N$. It is clear that the dependence of $R$ on $N$ can be approximated as a collinear function only under the extreme condition if $N$ is so tiny that the

influence of the nematicity is negligible to ***j*** and the usual van der Pauw analysis applies. Generally, $R$ does not bear a simple relation to $N$.

We note that van der Pauw (*SR5*), Montgomery (*SR6*) and others recognized this limitation and developed variants of the original van der Pauw method that are appropriate for measuring electronic nematicity. Unfortunately, these latter methods require either six planar samples of known and distinct orientation (*SR5*) or *a priori* knowledge of the principal axes (*SR6*), making them inappropriate for a study of a single thin film.

Nevertheless, we applied this method to analyze the resistance data shown in Fig. SF3a and calculated the longitudinal resistivity along the same [001] and $[1\bar{1}0]$ directions respectively (Fig. SF3c). The two $\rho(T)$ curves plotted in Fig. SF3c show no crossings, in stark contrast to the two R(T) curves in Fig. SF3a, but in qualitative agreement with the $\rho(T)$ curves in Fig. SF3b. This confirms that the crossing in Fig. SF3a is merely an artifact, due to the fact that the principal axes are not aligned with either the $a$ or $b$ axes. The quantitative values of $\rho(T)$ in Fig. SF3c at a fixed temperature, e.g. $T$ = 295 K, are fairly close to those of $\rho(T)$ in Fig. SF3b. The magnitude of the nematicity, determined by the difference between the two $\rho(T)$ curves, are nearly the same in Fig. SF3b and Fig. SF3c at 4.2 K, but gets underestimated in Fig. SF3c at elevated temperatures.

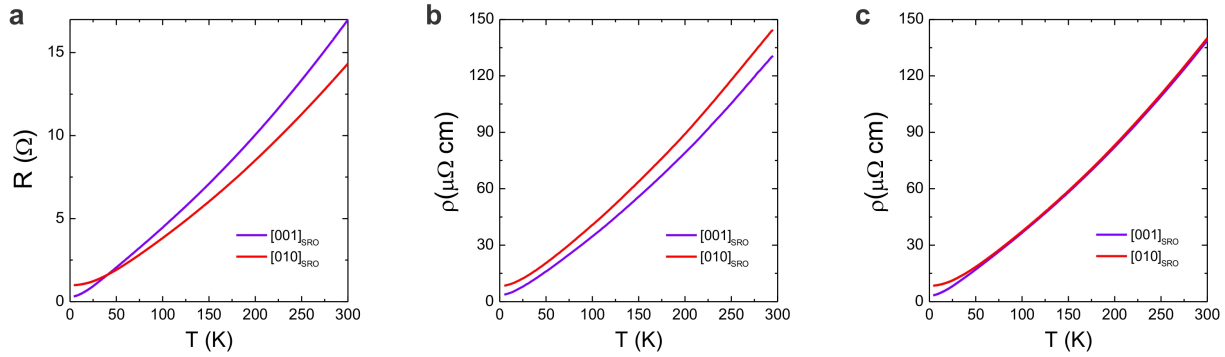


**Fig. SF3. A comparison of the van der Pauw and the sunbeam-pattern methods.** **a,** The longitudinal resistances of $Sr_2RuO_4$ grown on (110) $NdGaO_3$ were measured along [001] and $[1\bar{1}0]$ directions of $NdGaO_3$ respectively, by the van der Pauw method. **b,** On the same sample after being patterned by the sun-beam lithography pattern, the longitudinal resistivities were again measured. **c**, The longitudinal resistivity along [001] and $[1\bar{1}0]$ were calculated from the resistance data in **a**, based on the van der Pauw method generalized to anisotropic materials (*43*).

To avoid the complexity in analysis and modeling, the sun-beam method is clearly preferable. Moreover, for the more general case in which the principal axes do not align with the crystal $a$ or $b$ axis, e.g., in $Sr_2RuO_4$ films grown on LSAT (Fig. 1), the interpretation of the van der Pauw method gets less straightforward. For instance, if a principal axis is along the [110] direction of $Sr_2RuO_4$, then the measured $R_a = R_b$, misleading one to infer that the nematicity is zero. Therefore, the angular resolution of the sun-beam method is pivotal to ensure the accurate characterization of nematicity.

## 3. Robustness of superconductivity and electronic nematicity

The electronic nematicity is present in $Sr_2RuO_4$ films on both LSAT and $NdGaO_3$ substrates at room temperature and its magnitude increases with decreasing temperature. For the $Sr_2RuO_4$ film grown on a (110) $NdGaO_3$ substrate, superconductivity was observed at low temperatures with the onset $T_c$ = 0.9 K (Fig. SF4a). By adjusting the growth condition slightly off the optimal, we introduced more defects into the film and suppressed superconductivity so that no transition is observed (Fig. SF4c) down to 0.3 K. On the other hand, the angular dependence of $\rho_T(\phi)$ of both films manifest $180^0$ oscillations and possess a very similar "clover-leaf" shape when plotted in polar coordinates (Figs. SF4b and SF4d). This comparison clearly shows that the electronic nematicity in the normal state of $Sr_2RuO_4$ is robust against the disturbance caused by structural defects and the demise of the superconductivity. Nematicity, or a large nematic susceptibility, appears to be intrinsic to $Sr_2RuO_4$.

## 4. The substrate miscut is not the root cause of the observed nematicity

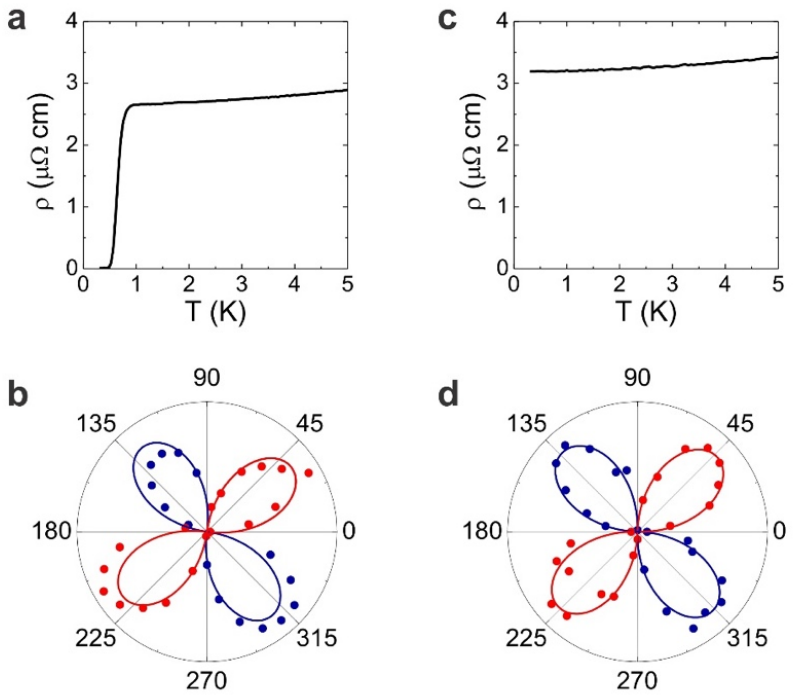


**Fig. SF4**. **The magnitude of nematicity is nearly the same in superconducting and non-superconducting $Sr_2RuO_4$ films.** **a,** the longitudinal resistivity $\rho(T)$ shows superconductivity with $T_c \approx 0.9$ K. **b,** $\rho_T(\phi)$ at $T$ = 295 K in the same sample, plotted in polar coordinates. **c,** $\rho(T)$ of a non-superconducting film with a higher residual resistivity. **d,** $\rho_T(\phi)$ of the non-superconducting film.

Restricted by the precision in the alignment during polishing, the surface of a substrate, e.g. LSAT, inevitably deviates from the ideal crystallographic {001} plane by a tiny miscut angle. The upper limit of the miscut for the substrates used is 0.2 degree. The atomic steps at the $Sr_2RuO_4$/LSAT and $Sr_2RuO_4$/$NdGaO_3$ interfaces, and the concomitant out-of-phase boundaries in the $Sr_2RuO_4$ film (*SF8*), in principle violate the $\mathbf{C}_4$ rotational symmetry. Traversing the steps and out-of-phase boundaries can increase the electronic scattering rate, so the in-plane resistivity could be larger in

that direction. In addition, note that $Sr_2RuO_4$ is a layered material and has a considerable in-plane vs. out-of-plane anisotropy so one could also increase the measured resistivity in the direction perpendicular to the substrate steps by picking up some *c*-axis component. If this were indeed the case, there should be a one-to-one correspondence between the step orientation and the orientation of the principal axes; resistivity should always be the lowest in the direction parallel to the steps.

This motivated us to explore whether the orientation and density of the atomic steps are related to the measured anisotropy in the $Sr_2RuO_4$ films. Since the miscut varies randomly from one substrate to another, the resulting atomic steps vary in density and orientation. By choosing substrates with different miscut and synthesizing $Sr_2RuO_4$ films under identical conditions, we can make a one-on-one comparison between the orientation of the anisotropy and the miscut. Since traversing the steps and out-of-phase boundaries can only increase the electronic scattering rate, and consequently the longitudinal resistivity, the in-plane direction parallel to the atomic steps should correspond to the direction in which the resistivity $\rho(\phi)$ reaches its minimum $\rho^{min}$.

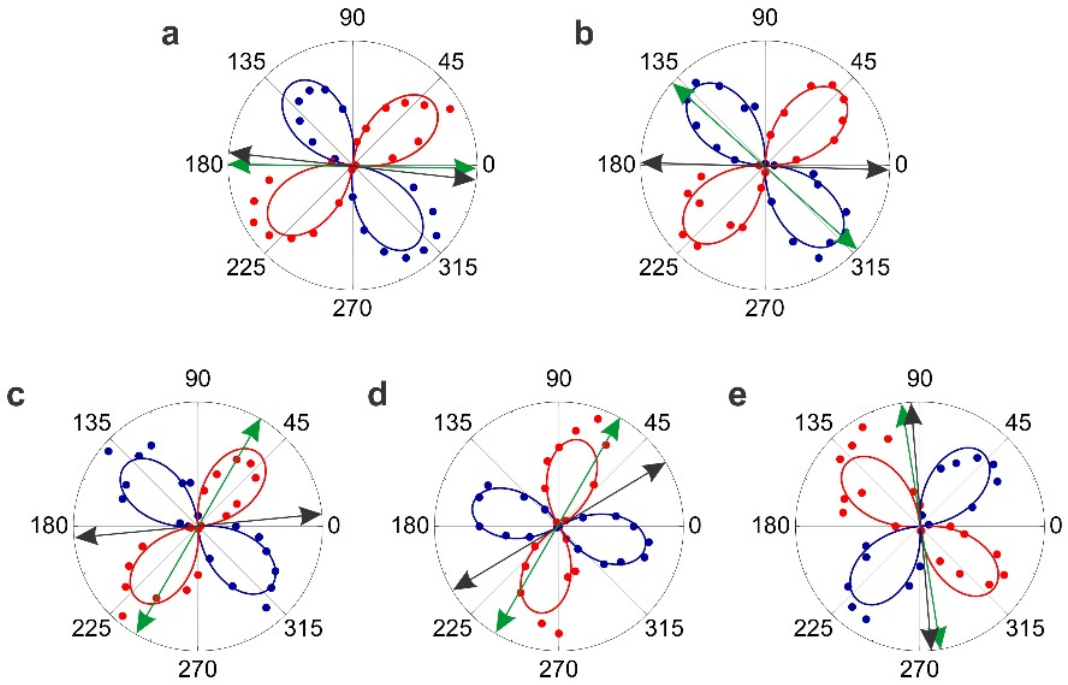


**Fig. SF5. In $Sr_2RuO_4$ films grown on (110) $NdGaO_3$ under identical growth conditions, the orientation of substrate steps (green arrows) does not coincide with the principal axis along which the resistivity is lowest (black arrows). a,** The miscut angle of the substrate is $\theta = 0.05^0$. **b,** $\theta = 0.06^0$. **c,** $\theta = 0.038\pm0.001^0$. **d,** $\theta = 0.140\pm0.002^0$. **e,** $\theta = 0.16\pm0.01^0$. The horizontal axis in all plots is along the direction with [001] the shorter lattice constant of the perovskite subcell in the $NdGaO_3$ substrate and the shorter in-plane lattice constant of the $Sr_2RuO_4$ film.

The direction and magnitude of the substrate miscut was measured by XRD using the technique outlined in Ref. *SR9*. In Fig. SF5, we show the measured orientation of the atomic steps, denoted by the green arrows, for five $Sr_2RuO_4$ films grown on (110) $NdGaO_3$ substrates. (The horizontal

axis in all plots is aligned with the [001] axis of $NdGaO_3$, i.e., it is in the direction with the shorter lattice constant of the perovskite subcell in the $NdGaO_3$ substrate and the shorter in-plane lattice constant of $Sr_2RuO_4$ film.) For comparison, the orientation of the principal axis along which the resistivity is lowest, i.e., the angle corresponding to $\rho^{min}(\phi)$, is indicated by the black arrows. It is clear there is no one-to-one correspondence between the orientations of substrate steps and the direction of $\rho^{min}$ (which would correspond to the nematic director).

Moreover, an even stronger argument against this model is its dramatic failure to account quantitatively for the magnitude of the observed effect. In principle, given the large out-of-plane vs. in-plane resistivity anisotropy in $Sr_2RuO_4$ (of the order of 1,000:1), the substrate miscut could cause some admixture of the *c*-axis resistivity if the current is running along the miscut direction. To estimate the magnitude of this effect, one needs to know the miscut angles, so these were measured and are indicated in the caption to Fig. SF5 for each of the five films. The smallest of these is $\theta = 0.038 \pm 0.001^0$ (Fig. SF5c) and in this case, the 'step model' would predict $N = 0.03\%$, three orders of magnitude less than what we see. And even for the largest miscut value, $\theta = 0.16 \pm 0.01^0$ (Fig. SF5e), the predicted $N$ would be less than 1%, still too low by a factor of 40. The details of this quantitative comparison are provided below.

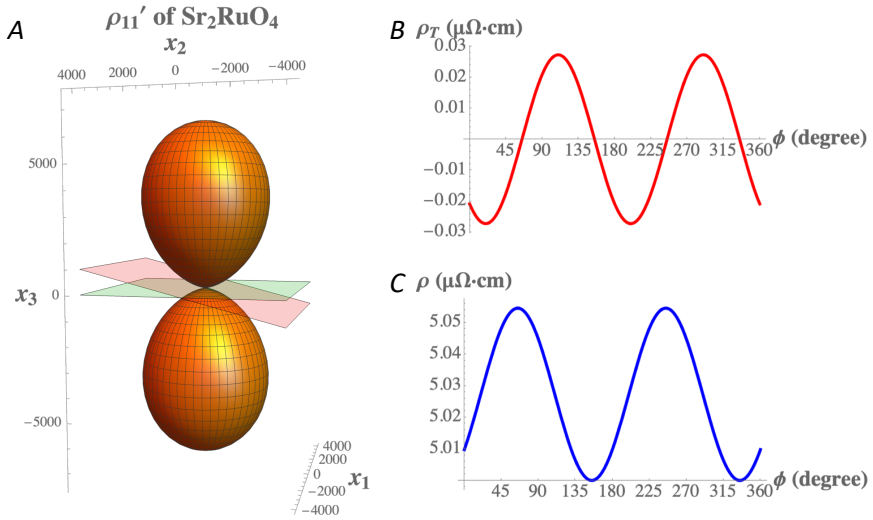


**Fig. SF6. Calculated effect of the misorientation of the substrate on $\rho_T(\phi)$ and $\rho(\phi)$.** (*A*) the calculated longitudinal resistivity of $Sr_2RuO_4$ in units of μΩ·cm. The green plane shows how a substrate precisely parallel to (001) would cut this figure; the case for a misoriented substrate is depicted by the red plane. The calculated transverse resistivity (*B*) and longitudinal resistivity (*C*) in a plane misoriented by $0.16^0$ from (001).

In this analysis we assume that $Sr_2RuO_4$ is not an electronic nematic and calculate the angular dependence of the longitudinal resistivity ($\rho(\phi)$ or $\rho'_{11}$ in tensor form) and transverse resistivity ($\rho_T(\phi)$ or $\rho'_{21}$ in tensor form) expected in a perfect epitaxial (001)-oriented $Sr_2RuO_4$ film due solely to a miscut of the underlying substrate. With space group $I\frac{4}{m}mm$ (*36*), the form of the resistivity tensor for $Sr_2RuO_4$ is $\rho_{ij} = \begin{pmatrix} \rho_{11} & 0 & 0 \\ 0 & \rho_{11} & 0 \\ 0 & 0 & \rho_{33} \end{pmatrix}$. At ~8 K, $\rho_{11} \approx 1\ \mu\Omega \cdot$ cm and $\rho_{33} \approx$

$1{,}400\ \mu\Omega \cdot \text{cm}$ in $Sr_2RuO_4$ single crystals and for temperatures < 20 K the ratio of $\frac{\rho_{33}}{\rho_{11}}$ is approximately constant with a value of 1,400. *(SR10)* In the calculation that follows we use $\rho_{11} \approx 5\ \mu\Omega \cdot \text{cm}$ and $\rho_{33} \approx 5 \times 1{,}400 = 7{,}000\ \mu\Omega \cdot \text{cm}$ for $Sr_2RuO_4$ to make the results easy to compare to Fig. 1*E* and *F* and Fig. 2*C* and *D*. These higher values of $\rho_{11}$ and $\rho_{33}$ can be considered to result from increased disorder or a higher temperature — about 32 K for the $Sr_2RuO_4$ single crystal. *(10)* The quantitative effect of misorientation on the magnitude of *N* depends solely on the ratio of $\rho_{33}$ to $\rho_{11}$.

The anisotropy of the longitudinal resistivity of $Sr_2RuO_4$ over all directions, not just those in the (001) plane, can be seen by plotting $\rho'_{11}(\theta, \phi)$ as a function of spherical angles $\theta$ and $\phi$. This is achieved using the tensor equation $\rho'_{ij} = a_{ik}a_{j\ell}\rho_{k\ell}$ with $a_{11} = \sin(\theta)\cos(\phi)$ , $a_{12} = \sin(\theta)\sin(\phi)$ , and $a_{13} = \cos(\theta)$ . A three-dimensional plot of the longitudinal resistivity, $\rho'_{11}(\theta, \phi)$, of $Sr_2RuO_4$ plotted as a function of direction with respect to unit vectors $x_1$, $x_2$, and $x_3$ parallel to the crystallographic axes *a*, *b*, and *c*, respectively, is shown in Fig. SF6*A*. It is evident that the anisotropy in $Sr_2RuO_4$ is very high and this is why utilizing well-oriented substrates and precisely establishing their misorientation is so important in this study. For a perfectly oriented (001) substrate, illustrated in Fig. SF6*A* by the green plane, the longitudinal resistivity in the (001) plane of the substrate would be a perfect circle and the transverse resistivity would be zero. When the substrate is misoriented, as schematically indicated in Fig. SF6*A* by the red plane, the in-plane resistivity becomes peanut shaped with principal axes aligned along the direction of misorientation. This is accompanied by the transverse resistivity becoming non-zero. The calculated dependence of the transverse resistivity, $\rho_T(\phi)$, and longitudinal resistivity, $\rho(\phi)$, in the plane of a $Sr_2RuO_4$ film that is misoriented by $0.16^0$ from (001) are shown in Figs. SF6*B* and *C*, respectively. It is evident that the magnitude of the calculated angular dependence is far smaller than the experimentally observed angular dependence seen in Fig. 1*E* and *F* and Fig. 2*C* and *D*.

## 5. Temperature dependence of $\rho$ and $\rho_T$

Representative plots of the temperature dependence of $\rho$ and $\rho_T$ for the $Sr_2RuO_4$ film grown on LSAT substrate are shown in Fig. SF7. The three angles $\phi$ are chosen so that $\rho(\phi)$ is at the maximum ($70^0$), middle ($110^0$), and minimum ($160^0$), see Fig. 1d and 1f for the $\rho(\phi)$ plot. It is clear from Fig. SF7 that $\rho(T)$ is parabolic, in contrast to the nearly-linear $\rho_T(T)$ behavior. This difference is also illustrated in Fig. SF7c. Apparently, the ratio $\rho/\rho_T$ is not constant, unambiguously showing that $\rho$ and $\rho_T$ are two independent physical quantities.

The correlation between $\rho$ and $\rho_T$ is given by the equations (1) and (2) in the main text. One consequence following these equations is the prediction that $\rho_T{}^0 = \Delta\rho = (\rho_{max} - \rho_{min})/2$. Here, at every temperature, $\rho_{max} = \rho(\phi = 70^0)$ and $\rho_{min} = \rho(\phi = 160^0)$, respectively. Meanwhile, $\rho_T{}^0$ corresponds to $\phi = 110^0$, the angle at which $\rho(\phi)$ reaches the average $\bar{\rho}$ while $\rho_T(\phi)$ reaches the maximum (see Fig. 1 in the main text). Therefore, it can be inferred that $\rho_T(\phi = 110^0) = (\rho(\phi = 70^0) - \rho(\phi = 160^0))/2$. Indeed, this non-trivial relation is clearly confirmed in Fig. SF7d. This is additional strong evidence that the unusual transverse resistivity $\rho_T$ originates from the electronic nematicity.

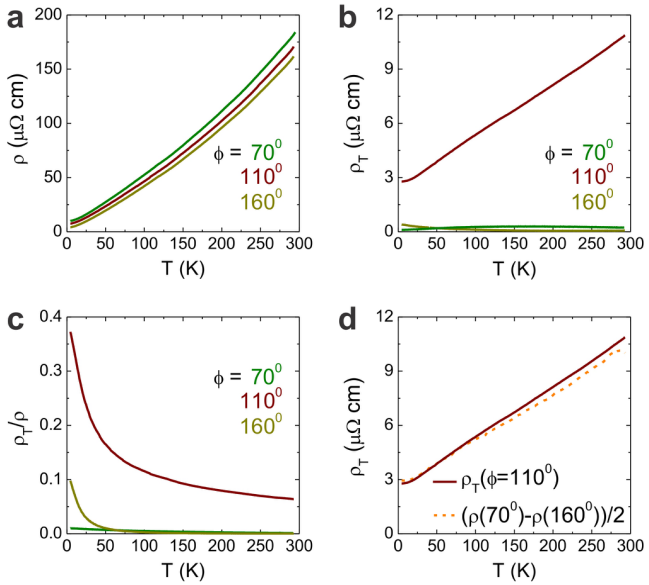


**Fig. SF7. Temperature dependence of $\rho$ and $\rho_T$ of the $Sr_2RuO_4$ film on LSAT substrate.** **a,** the longitudinal resistivity $\rho(T)$ at three angles corresponding to the maximum ($70^0$), middle ($110^0$), and minimum ($160^0$) of $\rho(\phi)$. **b,** $\rho_T(T)$ at these three angles. **c,** the ratio $\rho/\rho_T$ is not a constant, showing that $\rho_T$ is indeed not proportional to $\rho$, thus ruling out the possibility that the observed transverse voltage is due to misalignment of the voltage contacts. **d,** $\rho_T(\phi=110^0)$ is essentially equal to $(\rho_T(\phi=70^0) - \rho_T(\phi=160^0))/2$, as expected from equations (1) and (2). This shows that the origin of the transverse voltage is the anisotropy of $\rho$(T), i.e., the actual or incipient electronic nematicity.

## 6. Ruling out the artifacts of lithography: $\rho_T(\phi)$ in the control-sample Ti film

In order to test the (unlikely) possibility that our lithography and measurements may be the cause of the observed angular oscillations in $\rho_T(\phi)$, we performed a full ARTR study of a thin Ti film, chosen as a control sample. Ti is a well-known conventional metal and should not be an electronic nematic. Thus, for the Ti film, $\rho_T(\phi)$ should not oscillate with $\phi$; rather, it should be zero at every angle, by symmetry. Whether or not this is observed in our experiments is a decisive test of our ARTR methodology and of any artifacts due to lithography and measurement technique.

A 16 nm thick polycrystalline Ti film was deposited on (001) Si substrate by e-beam evaporation and patterned by the standard photolithography to form the sun-beam pattern as shown in Figs. 1a and 1b in the main text. ARTR measurements were carried out on the patterned Ti film, following exactly the same procedure as for the $Sr_2RuO_4$ films, in particular using the same lithography mask and the same measurement setup. To compare Ti and $Sr_2RuO_4$ films on the same footing, we normalized the measured $\rho_T(\phi)$ by the corresponding average longitudinal resistivity $\bar{\rho}$ for Ti and $Sr_2RuO_4$ films, respectively. The results are shown in Fig. SF8. Apparently, $\rho_T(\phi)$ in the Ti film shows no oscillations and is equal to zero within the experimental uncertainty. This is in stark contrast to $\rho_T(\phi)$ in the $Sr_2RuO_4$ film. Therefore, it seems quite definite that our lithography and measurement methodology are not the cause of the observed breaking of the rotational symmetry in $Sr_2RuO_4$ films.

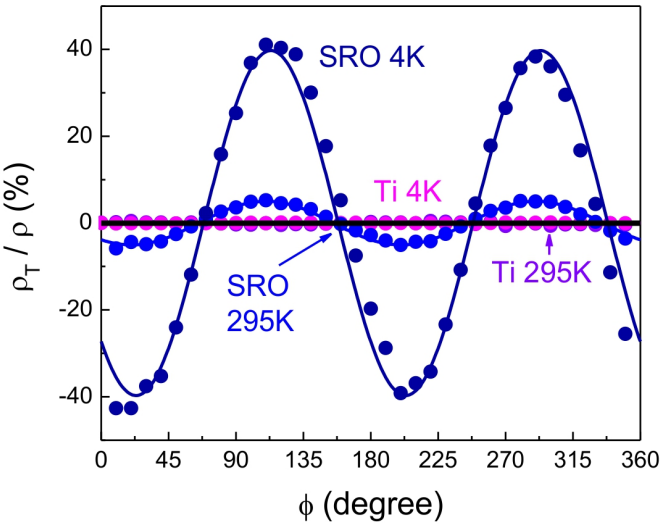


Fig. SF8. **Comparison of $Sr_2RuO_4$ with the Ti control sample.** In Ti film, $\rho_T(\phi)$ shows no angular oscillations at $T = 295$ K (purple dots) nor at $T = 4$ K (magenta dots). This is in stark contrast to $\rho_T(\phi)$ of the $Sr_2RuO_4$ film grown on the LSAT substrate ($T = 295$ K, lighter blue dots; $T = 4$ K, darker blue dots). The measured $\rho_T(\phi)$ is normalized by the average longitudinal resistivity $\bar{\rho}$ for the respective films, in order to facilitate the comparison. The solid lines are the best fits to $\rho_T(\phi) = \rho_T^0 \sin[2(\phi-\alpha)]$ for experimental data in the corresponding color. The solid black line stands for $\rho_T(\phi)/\bar{\rho} = 0$.

## Supplementary references


1. H. P. Nair *et al.*, Demystifying the growth of superconducting $Sr_2RuO_4$ thin films. *APL Materials* **6**, 101108 (2018).
2. W. R. Busing, H. A. Levy, Angle calculations for 3- and 4- circle X-ray and neutron diffractometers. *Acta Cryst.* **22**, 457 (1967).
3. Chinkyo Kim, "Strain Relaxation Mechanism of Semiconductor Thin Films." PhD Thesis, University of Illinois, Urbana (1998).
4. L. J. van der Pauw, A method of measuring specific resistivity and Hall effect of discs of arbitrary shape. *Philips Res. Rep.* **20**, 220–224 (1958).
5. L. J. van der Pauw, Determination of resistivity tensor and Hall tensor of anisotropic conductors. *Philips Res. Rep.* **16**, 187–195 (1961).
6. H. C. Montgomery, Method for measuring electrical resistivity of anisotropic materials. *J. Appl. Phys.* **42,** 2971–2975 (1971).
7. J. Wu, A.T. Bollinger, X. He, I. Božović, Spontaneous breaking of rotational symmetry in copper oxide superconductors. *Nature* **547**, 432-435 (2017).
8. M. A. Zurbuchen *et al.*, Morphology, structure, and nucleation of out-of-phase boundaries (OPBs) in epitaxial films of layered oxides. *J. Mater. Res.* **22** 1439–1471 (2007).

9. M. A. G. Halliwell, S. J. Chua, Determining substrate orientation using a high-resolution diffractometer. *Journal of Crystal Growth* **192**, 456-461 (1998).

10. N. E. Hussey, A. P. MacKenzie, J. R. Cooper, Y. Maeno, S. Nishizaki, and T. Fujita, Normal-state magnetoresistance of $Sr_2RuO_4$. *Physical Review B* **57**, 5505–5511 (1998).